

3D FINITE ELEMENT ANALYSIS IN DRILLING OF AA7075 REINFORCED WITH NANO SILICON CARBIDE PARTICLES

The Aluminium alloy 7075 (AA7075) reinforced with nano Silicon Carbide particles (nSiCp) has attractive applications in aerospace, automobile, aircraft, turbine blades and electronics substrates because of its excellent properties such as strength, stiffness, corrosion resistance, wear properties and strength to weight ratio. These modern-day industries use conventional operations like drilling, milling to get the required shape and size in order to ease the assembly process. Whereas, the dimensional accuracy of the drilled hole without any defect is vital to ensure the strength of the joint. However, drilling the aluminium nanocomposite is quite challenging due to its heterogenic properties, which requires sufficient knowledge of selecting the appropriate machining parameter setting and high-end strategies to achieve good surface finish, superior hole quality and dimensional accuracy. However, the drilling process is mainly influenced by the quality of the machine, drill tool geometry, tool material, cutting velocity and feed rate. This research aims to investigate the machinability of the fabricated aluminium nanocomposite by conducting experimental drilling tests. In addition, a 3D Finite Element Model (3D FEM) was developed to simulate the drilling process for understanding the influence of machining parameters on critical thrust forces, chip formation, chip morphology, stress and hole quality. The experimental results agreed well with the 3D FEM simulation results in the correlation study, which ensures the accuracy and reliability of the developed 3D FEM. The study also recommends to use low feed rate and higher cutting velocity for reducing the critical thrust force during drilling.

Keywords: Aluminium nanocomposite; nSiCp; Drilling; Thrust force; Chip morphology; 3D FEM

1. Introduction

Aluminium nanocomposite has found wide-ranging applications as functional and structural materials due to its superior properties, which increases the demand for it in the automobile, aerospace and aircraft industries. The aircraft components such as aircraft fittings, fuselage for military aircraft, aircraft wings, mould tools, fuse parts, nozzles and flow valves, missile parts, shafts, worm gears, bike frames, wheel sprockets and brake discs are manufactured with AA7075. This creates the attention and necessity for the researchers to perform an investigation on the machinability of aluminium nanocomposite [1-3]. It has been expected that the average usage of aluminium material in a car will extend to 25% by the year 2025, the 1970s to today it is 15.2% compared to 3.5% before the 1970s [4]. The aluminium nanocomposite is categorized under aluminium-based Metal Matrix Composites (MMC's) which possess better toughness, ductility, high stiffness, good tensile strength and higher fracture toughness even at different operating conditions. The aluminium nanocom-

posites are made by incorporating nano-sized SiC particles (<100 nm) inside the matrix of AA7075 as reinforcement to enhance the mechanical behaviour of AA7075.

In aerospace, automotive, and other modern industries, drilling is the most challenging machining process, because a large number of holes are required for riveting and for making assembly joints of the structural parts. For example, the Airbus A300 and Boeing 747 need about 1 million and 3 million holes respectively [5]. However, the quality of the holes drilled is very much important for guaranteeing the strength of the assembled joint. The aluminium nanocomposite is nonhomogeneous and harder to drill due to the reinforcement material. Hence, the choice of appropriate drilling parameters and good machining strategies are required to ensure the quality of the drilled hole and its reliability [6-8]. The most challenging problems encountered during the machining of MMC's are burr formation, poor surface finish, errors in circularity, stress concentration, dimensional inaccuracy, tool wear and chip built-up edge. Therefore, significant investigations and research are mandatory which is carried

¹ SCHOOL OF ENGINEERING AND TECHNOLOGY, SURYA GROUP OF INSTITUTIONS, VIKIRAVANDI – 605 652, TAMILNADU, INDIA

* Corresponding author: prakashc@suryagroup.edu.in



out to evaluate the influence of parameters such as tool coating material, cutting parameters, tool vibration and tool geometry [9]. Hence, ensuring the dimensional accuracy and reliability of the components machined can be achieved only by minimizing the drilling-induced damages stated above [10]. These requirements encourage the researchers to do an investigation on drilling of aluminium-based MMC's [11]. Machining a hole with extreme quality is vital to avoid crack initiation in the airframe structure, which could lead to more part rejection at the assembly stage. Moreover, this increases the production time and product cost [12].

To overcome these machining complications, experimental studies are required, but it is time-consuming and costly; particularly for investigating a wider machinability metric (i.e. with various combinations of machineries, material, drill geometry, tool coatings and machining conditions) [13,14]. In addition to this, the accuracy and reliability of the experimental results predominantly rely on the utilised machine quality and the testing equipment during experimental machining. Hence, the researchers and industries wish to use 3D Finite Element Method (3D FEM) for investigating the machining of conventional materials and composites. Using 3D FEM the complex drilling process is simulated in 3D to visualize and understand the drilling process and chip creation.

Giasin et al. [15] performed an investigation on evaluating thrust forces, hole dimensional accuracy and quality using experimental and FEM in the drilling of AA2024. The results reveal that the drilling parameters have a major influence on the thrust force and quality of the drilled hole. Muhammad Aamir et al. [11] reviewed and documented the investigations carried out in recent times on the drilling of quality holes in aluminium alloys for aerospace applications. Drilling operation is suggested with a higher cutting speed and lower feed rate to minimize the thrust forces. Moreover, the usage of a Drill bit with helix angle 30° and higher point angle 130° to 140° is preferred to minimize the machining defects and thereby enhance the quality of the component machined. Nafiz Yaşar [16] used FEM to simulate the drilling operation in AA7075 material and reported the influence of cutting velocity and feed rate on the generated thrust force. The author also reported that thrust forces increase while drilling with a higher feed rate. AA7075/SiCp composites are utilised by the current modern-day industries because of their high tensile strength and wear resistance. SiC-reinforced metal matrix composites are preferred since it is having very good refractoriness and high abrasion resistance. The improvement of tensile strength was observed by adding SiC particles as reinforcement while casting the material [17].

Sajad Rasaei et al. [18] predicted the flow stress by using the basic and modified JC constitutive equations and evaluated the ability as well as reliability of FE models. Moreover, correlation studies with the experimental results are also carried out. Paresh Kumar et al. evaluated the mechanical properties and the surface roughness by drilling of Al7075 reinforced with SiC. The investigation also reveals that the lower feed rate gives a better surface finish in drilling the composite [19].

Senthil Babu et al. [20] performed parametric analysis on drilling of aluminium-based composite reinforced with SiC and WC. The author suggested performing with feed rate = 0.05 mm/rev , $N = 1000 \text{ rpm}$ and drill tool point angle = 128° to minimize the thrust force-induced damages and to enhance the quality of the holes drilled. The thrust forces rise considerably while increasing the feed rate. Samadhan Deshmukh et al. [21] reviewed on machinability of aluminium-based MMC's to understand the extent of research and scope for future research on cutting tool technology. The authors also explain the need to explore on implementation of FEM, in predicting the mechanical properties and response of MMC's while machining. The heterogeneity due to the reinforcement of SiC particles makes the machinability of the MMC's difficult and causes extensive tool wear. Hence, applications of aluminium-based MMC's are extensively hindered due to the difficulties associated with producing defect-free components with higher tolerance and surface finish [22].

The computational techniques used to simulate machining processes are Discrete Element Method (DEM), Smoothed Particle Hydrodynamics (SPH), Particle Finite Element Method (PFEM), Material Point Method (MPM) and Finite Element Method (FEM/FEA). The DEM technique is basically used to analyze the behaviour of granular, rock materials under load conditions. It is also used by the pharmaceutical and chemical industries to understand the behaviour of chemicals at the microscopic level. PFEM and SPH techniques are used for solving melting problems with phase change and larger deformation problems and these are alternate for FEA under certain situations. MPM technique is mainly used to analyse geotechnical problems which is effective for characterizing soil and structure interaction.

Yong He et al. investigated the suitability of DEM in predicting the cutting forces and chip morphology while performing orthogonal cutting in ductile iron [23] and the investigation suggests DEM to model heterogeneous materials. Geng et al. simulated the orthogonal cutting process using the Smoothed Particle Hydrodynamics (SPH) technique and reported that chip morphology is reasonable since it is a meshless method [24]. Carbonell et al. modelling 2D and 3D models to simulate the orthogonal machining process and reported that PFEM is good in providing good results in predicting the chip thickness, cutting forces and feed forces [25]. John investigated the capability of the MPM technique in simulating the orthogonal cutting process and suggested to refining the MPM to get good results [26]. Although the above techniques are available, they are not common in practice as it has limitations in modelling cutting problems.

The author of this research work Prakash C et al. [27-30] have presented a recent work focusing on 3D FEA (Finite Element Analysis) in drilling and slot milling of Glass Fiber Reinforced Polymer (GFRP), Carbon Fiber Reinforced Polymer (CFRP) composites to investigate the cutting forces, the process of chip formation and segregation, stress and chip morphology. This developed 3D FEM is a novel, fully-realistic numerical tool

which simulates the drilling process and assists the researchers in selecting appropriate process parameters to drill the composites. Prakash J et al. [31, 32] the co-author of this research article fabricated aluminium (AA7075) nanocomposite with various compositions and carried out mechanical characterization of the MMC's and also performed experimental micro drilling in the composite. The mechanical characterization studies reveal that AA7075 with 1.5% nSiCp composition possesses intrinsic and enhanced mechanical properties which suit wider applications, particularly in the automobile and aerospace industries. Our current research extends and suggests the usage of FRP and MMC composites in producing and replacing conventional metals with the light-weight composites for specific applications such as brake discs which also involve drilling, slot milling and end milling operations [33]. Currently, we are also investigating and evaluating the possibilities of replacing steel/cast iron chain sprockets with MMC/FRP composite.

From the literature and the author's earlier investigations, even though few 3D FEM-based machining simulation studies have been reported on drilling and milling [34] particularly in FRP's and MMC's the chip morphology-related studies were very limited in MMC's reinforced with nanoparticles. Furthermore, a clear understanding of the influence of machining parameters on critical cutting force, chip formation and segregation phenomenon, chip morphology and machining-induced damages are very much required to improve the performance of drilling. Moreover, there are no correlation studies on chip failure and chip morphology from an experiment Vs machining simulation using FEA [33,34].

The literature review also discloses that 3D FEM is not yet effectively developed to simulate the drilling operation for investigating the above details, particularly in MMC's. However, 3D FEM-based drilling simulation studies require an enormous amount of computation resources and excellent knowledge of good 3D modelling and machining mechanics; as the modern tools are highly complex in their geometry. In addition, the selection of suitable cutting velocity and feed for drilling the MMC influences the quality of the components machined. Hence, utmost care is needed in selecting the process parameters, which requires numerous experimental drilling trials for selecting the appropriate process parameters, which is more arduous. This necessitates developing 3D FEM for predicting appropriate cutting velocity and feed for making defect-free components.

Therefore, this research work devotes to developing a 3D FEM which is an excellent numerical tool for simulating and visualizing the drilling operation of AA7075 + 1.5% nSiCp Metal Matrix Composite (MMC). This drilling simulation study using experimental and 3D FEM methods exhibits and provides insight into the distinctiveness of the fabricated MMC and its deformation behaviour while drilling. The chip morphological studies provide vital evidence related to the deformation behaviour of the MMC during drilling, which also helps in understanding the failure behaviour of the MMC. The critical thrust force data is captured while performing experimental drilling and machining

simulation assists in making components with a higher degree of accuracy.

This research work also emphasizes the need and importance of 3D FEM in simulating the metal cutting and separation processes in drilling and for endorsing its advantages to researchers and industries. This 3D FEM drilling simulation analysis assists in selecting optimum machining parameter settings for evading the drilling-induced damages and eases in ensuring of manufacturing good quality components/products. The precision and the consistency of the 3D FEM drilling simulation results observed from this research work create curiosity for the authors for planning further to investigate machining the Fiber Reinforced Polymer (FRP), MMC's using tools with new geometry.

2. Methodology

In the current research work, AA7075 + 1.5% nSiCp MMC is fabricated and drilling experiments were carried out to investigate its machinability for proving the suitability of the composite for industrial applications. In addition, 3D FEM-based analysis is carried out and the drilling process is simulated. The outcome of this investigation reports the critical thrust force, chip morphology of the drilled chip, stress developed during drilling, chip formation and chip separation. The experimental and 3D FEM results were correlated for validating the accuracy of the FEM, which creates a pathway to select appropriate machining parameter settings for drilling the MMC to achieve defect-free components.

2.1. Workpiece material for drilling study

The MMC (AA7075 + 1.5% nSiCp) preferred for this research is fabricated by reinforcing with nano-sized (45-65 nm) SiC particles into AA7075 aluminium alloy matrix. The AA7075 matrix material shows good mechanical properties such as light-weight, high strength, good surface finish and better thermal stability. Similarly, the reinforcement material nSiCp also owns good mechanical properties such as high resistance to wear, low coefficient of thermal expansion, good thermal conductivity and high-temperature resistance. Hence, SiC-reinforced alloys and metals are mostly preferred in making nozzles and flow valves. Therefore, nSiCp is used as the reinforcement material in our research work for fabricating aluminium nanocomposite.

The Ultrasonic cavitation with stir-casting setup used for the fabrication of the composite is shown in Fig. 1. Using this setup the aluminium nanocomposite is fabricated in five different AA7075 + nSiCp compositions (nSiCp ranging from 0 to 2.5%). Furthermore, mechanical characterization studies were carried out and it is observed that out of five different compositions, the mechanical properties of aluminium nanocomposite with 985 grams of AA7075 + 15 grams of nSiCp (1.5% by weight) is excellent comparatively. Hence, based on the literature review and the earlier investigations [31] by the co-author, the composi-



Fig. 1. Ultrasonic cavitation with stir-casting setup [31]

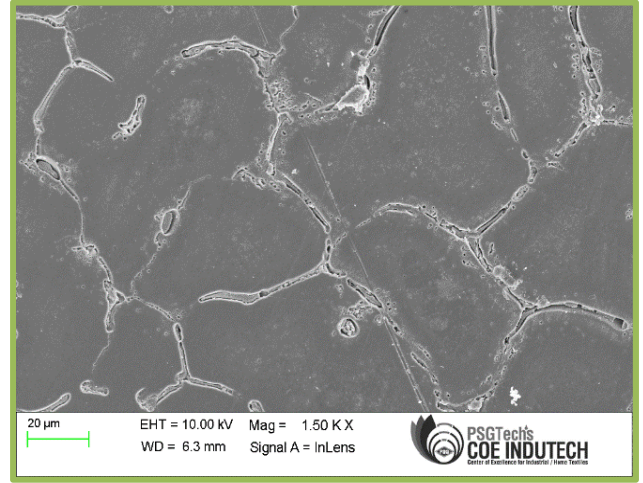


Fig. 2. FESEM micrograph of the composite [31]

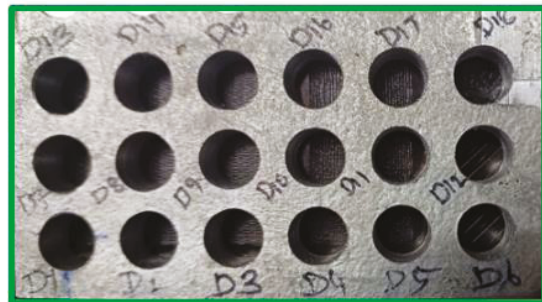
tion (AA7075 + 1.5% nSiCp) is preferred for this research work. This fabricated light-weight MMC is a very good alternative for steel. The former research by the co-author reveals the enhancement of the mechanical properties of AA7075 with 1.5% nSiCp. The mechanical properties of the fabricated nanocomposite such as tensile strength, hardness, impact strength, corrosion resistance and wear resistance are excellent [31]. TABLE 1 shows the composition of the fabricated aluminium nanocomposite used for drilling experimentation. Field Emission Scanning Electron Microscope (FESEM) image reveals the distribution of nSiCp in the preferred composition of aluminium nanocomposite in Fig. 2 [31].

2.2. Experimental setup and methods

The experimental drilling was completed in BMV 51 TC24 CNC vertical machining centre which has the capacity of 11 KW power and a maximum tool rotation speed of 6000 rpm. Fig. 3 displays the experimental setup which consists of the CNC vertical machining centre, drill tool, workpiece material and the tool dynamometer with data acquisition system. The TiAlN-coated solid carbide drill bit (shown in Fig. 3a) with the specifications given in TABLE 2 is used for experimental investigation. The selection of a drill bit with a helix angle 30° and a higher point angle of 130° to 140° is preferred for drill-



a) Drill tool



b) Workpiece - Aluminium nanocomposite (AA7075 + 1.5% nSiCp)



c) CNC Machining facility



d) Drill tool Dynamometer with Data-Acquisition setup

Fig. 3. Drilling Experiment setup

ing experimentation (particularly for composites) based on the previous research carried out by the authors and the literature review [11,20,27]. The drilling experiments were conducted at room temperature for different cutting velocities and feed rates as per the Experimental plan given in TABLE 3. The drilling parameters are selected with different combinations of spindle speed (N) ranging from 500 rpm to 3000 rpm and feed rate (f) ranging from 5 to 20 mm/min. The selection of machining parameter values is formulated based on the information obtained from the trial experiments and the literature review.

The chip morphology studies are carried out to evaluate the failure behaviour and machinability of the fabricated MMC. The higher cutting velocity with a lower feed can be preferred for experimental drilling to minimize the thrust forces and torque [11]. However, a low and moderate range of process parameters is

selected for the drilling experiments in the current research, only at which the chips collected are good to categorize for performing morphological studies and to investigate further [27,28]. Thrust forces are recorded using a SYSCON – strain gauge-based tool dynamometer and its lab view-based Data-Acquisition system which is presented in Fig. 3(d). The thrust force data is captured in the form of peak value analytically and also in the form of a graph (Thrust force Vs. Time) during the drilling operation. The temperature while performing the experimental drilling is captured at the cutting zone region and it is minimal in the range of 125° to 200°C. The drill tool temperature was monitored continuously with a noncontact type infrared temperature sensor as the current investigation is carried out in dry conditions without coolant.

TABLE 1

Composition of aluminium nanocomposite – AA7075 + 1.5% nSiCp (percentage by weight) [27,28]

Cr	Mg	Zn	Cu	Si	Mn	Ti	Fe	SiC	Al
0.2	2.4	5.7	2.0	0.3	0.1	0.1	0.22	1.5	Bal

TABLE 2

Properties and Geometric details of carbide twist drill [28]

Specifications / Description	Value(s) / Details	Specifications / Description	Value(s) / Details
Product Name	Twist drill	Coating material	TiAlN
Type of the Shank	Plain	Thickness of Coating (Microns)	2 to 4
Diameter of the tool (mm)	10	Max. Working Temperature (°C)	950
Total tool length (mm)	62	Colour of Coating Material	Reddish – violet – black
Length of the Shank (mm)	32	Hardness of the Drill (Hv)	3300
Length of the Flute (mm)	30	Density (kg/m ³)	11,500
Diameter of the Shank (mm)	10	Helix angle of the drill tool (°)	30
Drill Tool Material	Solid Carbide	Point angle of the drill tool (°)	130
Type	High-performance drill	Chisel edge radius (mm)	0.7
Number of flutes	02	Chisel edge angle of the drill tool (°)	135
Dimension style of the Drill	Metric	Lip relief angle of the drill tool (°)	12

TABLE 3

Experimental parameters in drilling of aluminium nanocomposite [11]

Drilling parameters	Value(s)
Spindle speeds, N (rpm)	250, 500, 1000, 1500, 2000, 3000
Cutting Velocity, V_c (m/min)	7.85, 15.7, 31.4, 47.1, 62.8, 94.2
Cutting Feed rate, f (mm/min)	5, 10, 20

TABLE 4

Mechanical properties of aluminium nanocomposite [19,31]

Specifications	Value (s)	Specifications	Value (s)
Modulus of Elasticity (GPa)	71	Tensile Strength (MPa)	285.64
Poisson's ratio	0.27	Yield Strength (MPa)	251
Thermal Expansion Coefficient, (1/K)	23.6 E-6	Ultimate Strength (MPa)	260.56
Thermal Conductivity (W/mK)	180	Shear Strength (MPa)	150.53
Specific heat (J/kg K)	880	Density of the composite (kg/m ³)	2790
Micro hardness (Hv)	136.4	Impact Strength (J)	14.2
Melting Temperature (K)	896	Corrosion rate (mm/year)	0.473

3D Finite Element Model data

Workpiece material	Aluminium nanocomposite
Tool material	Solid Carbide Twist Drill
Dimensions of the composite in FE Model	15 × 15 × 10 mm
Workpiece element type	C3D8R
No. of elements in composite	90,000
No. of nodes in composite	97,061
Average element size in composite	0.25 mm
Drill tool element type	C3D10M
No. of elements in drill tool	11,807
No. of nodes in drill tool	18,402
Average element size in drill tool	1 mm
Total number of elements & nodes in 3D FEM	1,01,807 & 1,15,463
Coefficient of Friction & type	0.5 & Coulomb Friction
Failure criteria	Johnson Cook Model

TABLE 6

Material constants for Johnson – Cook constitutive model of aluminium nanocomposite

A (MPa)	B (MPa)	n	m	C	Reference Temperature T (K)	Melting Temperature, T (K)	Damage Initiation
251	1443	0.749	1.571	0.0166	305	896	0.001

TABLE 7

Johnson – Cook damage parameters for aluminium nanocomposite

d_1	d_2	d_3	d_4	d_5
-0.77	1.45	-0.47	0	1.60

2.3. Finite element analysis

2.3.1. FEA Methodology

In the current work, the 3D Finite Element Model was developed in ABAQUS/Explicit to simulate and investigate the drilling process in the aluminium nanocomposite [36]. ABAQUS/Explicit can effectively handle the extreme nonlinear behaviour without any runtime termination of the FE solver, which facilitates much in performing machining simulations. 3D FE simulation trials are performed for different machining parameters to predict the maximum thrust force, chip formation and separation and chip morphology. The input details for the 3D FEM are given in TABLE 5 are incorporated to discretize the geometric model and to characterize the material behaviour of the tool and workpiece.

2.3.2. 3D FEM of MMC and Drill tool

The three-dimensional model of the twist drill is created with two flutes in CATIA V5 using the part module [37] (as shown in Fig. 4) and the tool nomenclature is given in TABLE 2. The workpiece model is created (as shown in Fig. 5) considering the mechanical properties of the aluminium nanocomposite which is given in TABLES 4, 6, 7. The twist drill is discretized with 11807 elements of C3D10M tetrahedron elements as it is

an appropriate element to discretize complex geometry with sharper edges and curvatures (as shown in Figs. 4, 5) with a good aspect ratio. The twist drill is considered as a rigid body in this investigation and it is assumed in such a way that it does not deform or wear. Assuming the drill tool has a rigid body is a com-

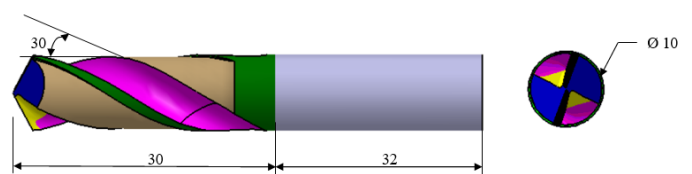


Fig. 4. Three dimensional model of the solid carbide twist drill

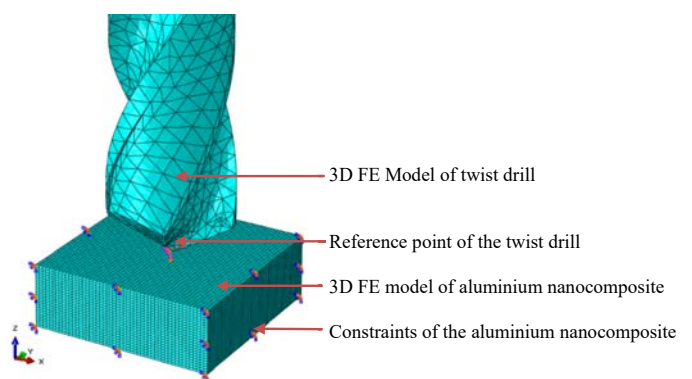


Fig. 5. Three dimensional Finite Element Model of drilling the aluminium nanocomposite

mon practice in most of the earlier studies significantly reduces the computational resources. The aluminium nanocomposite is meshed with 90,000 C3D8R eight-noded brick elements as it suits best for the regular geometry (Block shaped – as shown in Fig. 5). The mesh optimization studies are performed to optimise the running time of the FE solver without compromising the accuracy of the results.

2.3.2. Assumptions in developing 3D FEM

- The created 3D FEM is an Equivalent Homogeneous Model (EHM).
- The twist drill is considered a rigid body.
- The wear of the twist drill is not taken into account.
- The 3D FEM of the nanocomposite is a scaled model.
- Temperature effects were not considered in the current investigation, which is our future scope of study.

2.3.3. Load and Boundary conditions

The boundary conditions are defined realistically on all side faces of the MMC and constrained for all Degrees of Freedom (DoF's) (Encastre: $U1 = U2 = U3 = UR1 = UR2 = UR3 = 0$). The twist drill is constrained for all DoF's in X and Y, allowed to move along Z direction and can rotate with respect to Z axis ($U1 = U2 = UR1 = UR2 = 0$). In addition, translation motion (feed rate) and rotational velocity (Spindle speed) are applied to the reference point, RP (shown in Fig. 2). The feed rate and cutting velocity are given as FE inputs (machining parameters given in TABLE 3) [27,30]. Using the trial simulation study we have tested with larger specimen sizes too (Farther edges constrained model) and the correlation of results doesn't show much difference in thrust forces. This ensures that, scaled 3D FEM is reliable in predicting the results.

2.3.4. Failure and Damage model for the composite

The Johnson cook (J-C) failure criteria are used for our 3D Finite Element Analysis (3D FEA) as it is a proven failure model in simulating the machining processes of conventional metals and MMC's [33,35]. The Johnson's cook failure model for the aluminium nanocomposite was incorporated which is available in the material model of the ABAQUS software. The J-C parameters given in Table 6 characterize the mechanical behaviour of the MMC. The J-C failure criteria are represented by the following equation.

$$\text{Flow stress, } \sigma = (A + B\varepsilon^n) \left(1 + C \ln \frac{\varepsilon_1}{\varepsilon_0} \right) \left[1 - \left(\frac{T - T_r}{T_m - T_r} \right)^m \right] \quad (1)$$

In which, the constants A, B, C, n, m, T are listed in TABLE 3.

The damage criteria are incorporated into the 3D FEM to initiate the chip formation and separation when the material reaches the criteria value (given in TABLE 7).

2.3.5. Tool – Workpiece interaction model

The contact and friction properties are incorporated into the 3D FEM in the interaction module of the ABAQUS. The general contact algorithm in ABAQUS software is used to characterize the surface erosion (chip removal) in drilling the aluminium nanocomposite. The surface-to-surface contact algorithm with normal behaviour and hard contact concepts was used. The coulomb friction concept with a coefficient of friction of 0.5 [33] is used to depict the friction properties at the tool-workpiece interface.

$$\tau_n = \mu \sigma_n \quad (2)$$

2.3.6. Solution & Post processing

The created 3D FEM is solved with the FE solver in ABAQUS/Explicit. The running time of the FE Analysis depends on the total time step and no of steps defined in the analysis. Once the problem is solved, the FE solver saves the results in the form of filename.odb format which consists of all the predicted output such as cutting forces, chip formation, stress, strain etc. The odb file can be opened in ABAQUS viewer module for visualising the simulated results in the form of video and graphical images. The results were compiled in the required format and presented.

3. Results and discussion

3.1. Thrust force

The thrust force is generated in the feed direction (F_z) of the twist drill while drilling. The magnitude of this thrust force mainly depends on the hole diameter, strength properties of the workpiece, geometry of the twist drill, machining environmental conditions, feed rate and spindle speed etc. This critical force extremely affects the chip formation, chip morphology which directly influences on accuracy of the machined components. Therefore, there is a need to perform investigation studies on the developed thrust forces while drilling the aluminium nanocomposite. Moreover, capturing the actual magnitude of the critical thrust force is challenging, which fully depends on the accuracy, repeatability and reliability of the utilised machines and testing equipment for performing the experimental studies. The FEA investigations and literature studies conclude that chip thickness, chip morphology and the chisel edge of the drill tool are the influencing factors for the generation of higher thrust force values in drilling the MMC's [38].

Fig. 6(a)-(b) discloses how thrust force fluctuates and it is in a cyclic pattern, which is due to the reinforcements in the

composite laminate and other machining conditions. Fig. 6(a)-(b) also shows the captured thrust force signal while drilling the aluminium nanocomposite which discloses the four stages of the drilling process such as penetration of the tooltip, complete engagement of cutting lip with composite, tooltip exit and complete exit of cutting lips. However, during the drilling stages 1 and 3 the thrust forces detected are in increasing and decreasing trend respectively, because during these stages the drill tool will not completely engage with the workpiece. In stage 2 the thrust

force (F_z) captured is maximum when compared to other stages and more fluctuation is observed as the drill tool engaged completely with the composite and also due to the coupled effect of reinforcement material. However, the observed minimal fluctuation is because of the nSiCp reinforcement and heterogeneous properties of the nanocomposite. This maximum thrust force, F_z recorded is termed as the critical thrust force, above which the machining-induced damages will be predominant while drilling the aluminium nanocomposite.

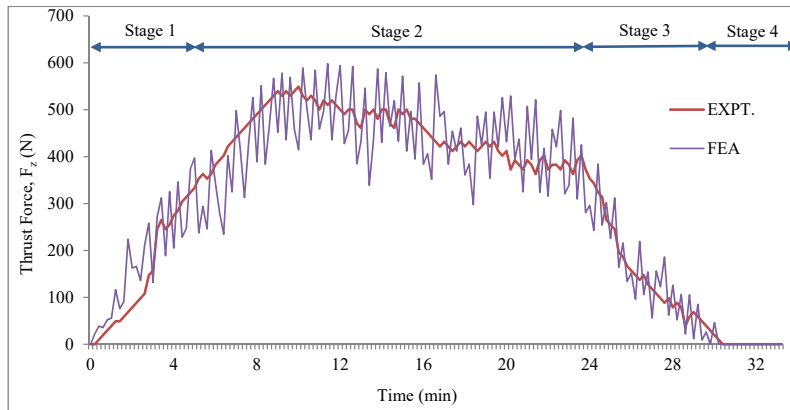


Fig. 6. (a) Comparison of experimental and 3D FEA data of thrust force (F_z) in Drilling of aluminium nanocomposite at $V_c = 15.7$ m/min, $N = 500$ rpm and Feed rate, $F = 20$ mm/min

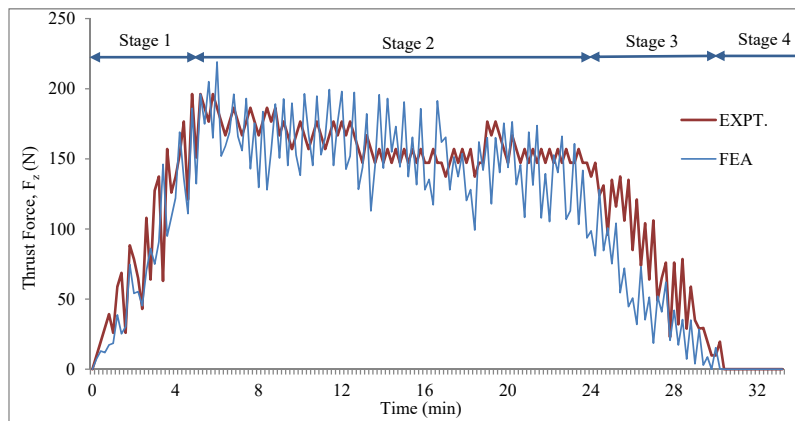


Fig. 6. (b) Correlation of experimental and 3D FEA data of thrust force (F_z) in Drilling of aluminium nanocomposite at $V_c = 94.2$ m/min, $N = 3000$ rpm and Feed rate, $F = 20$ mm/min

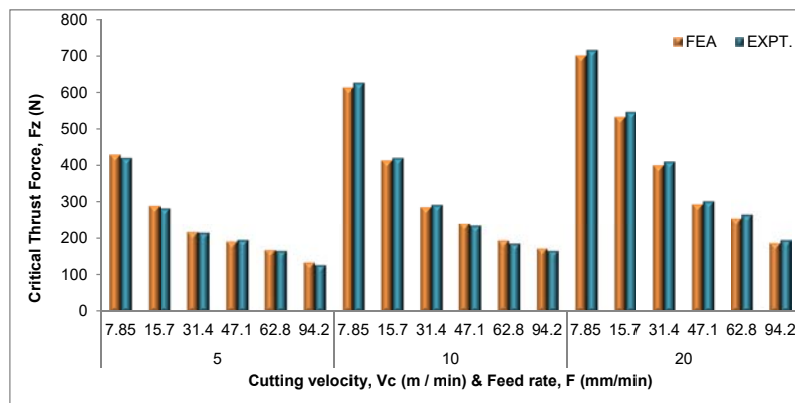


Fig. 7. Correlation of experimental and 3D FEA results – Critical thrust force (F_z) in Drilling of aluminium nanocomposite V_s Cutting velocity and Feed rate

TABLE 8

Critical thrust force data for different combinations of cutting velocity and feed rate.

Feed rate, f (mm/min)	Cutting Velocity, V_c (m/min)	Critical Thrust force (F_z)	
		Expt. (N)	FEA (N)
5	7.85	422	431
	15.7	284	289
	31.4	216	218
	47.1	196	192
	62.8	167	169
10	94.2	128	135
	7.85	628	615
	15.7	422	415
	31.4	194	288
	47.1	235	242
20	62.8	186	195
	94.2	167	173
	7.85	716	701
	15.7	549	536
	31.4	412	402
20	47.1	304	296
	62.8	265	254
	94.2	196	188

Figs. 6 and 7 display the magnitude of the thrust force acquired from experimental and 3D FE simulation results. This fluctuating thrust load is because of the interaction of the cutting edge with the nSiCp reinforcement and also due to the inhomogeneity property of the aluminium nanocomposite [39]. Fig. 7 displays the correlation of the critical thrust force data obtained from drilling experiments and 3D FE simulation studies for the respective cutting velocity and feed rate. When the drilling is made with higher cutting velocity, the developed critical thrust forces are observed to be relatively minimal [40,41]. Hence, it is recommended to do the drilling process at a higher cutting velocity or lower feed per tooth to minimize the drilling-induced damages because of the thrust force. The experimental critical thrust force results agreed excellently with the results captured from the 3D FEM drilling simulation. Fig. 7 also shows very minimal deviation of 5 to 10% in the numerical and experimental data.

3.2. Stress

Shear stress plays a vital role in the chip formation phenomenon while drilling MMC. While drilling, the chip is cre-

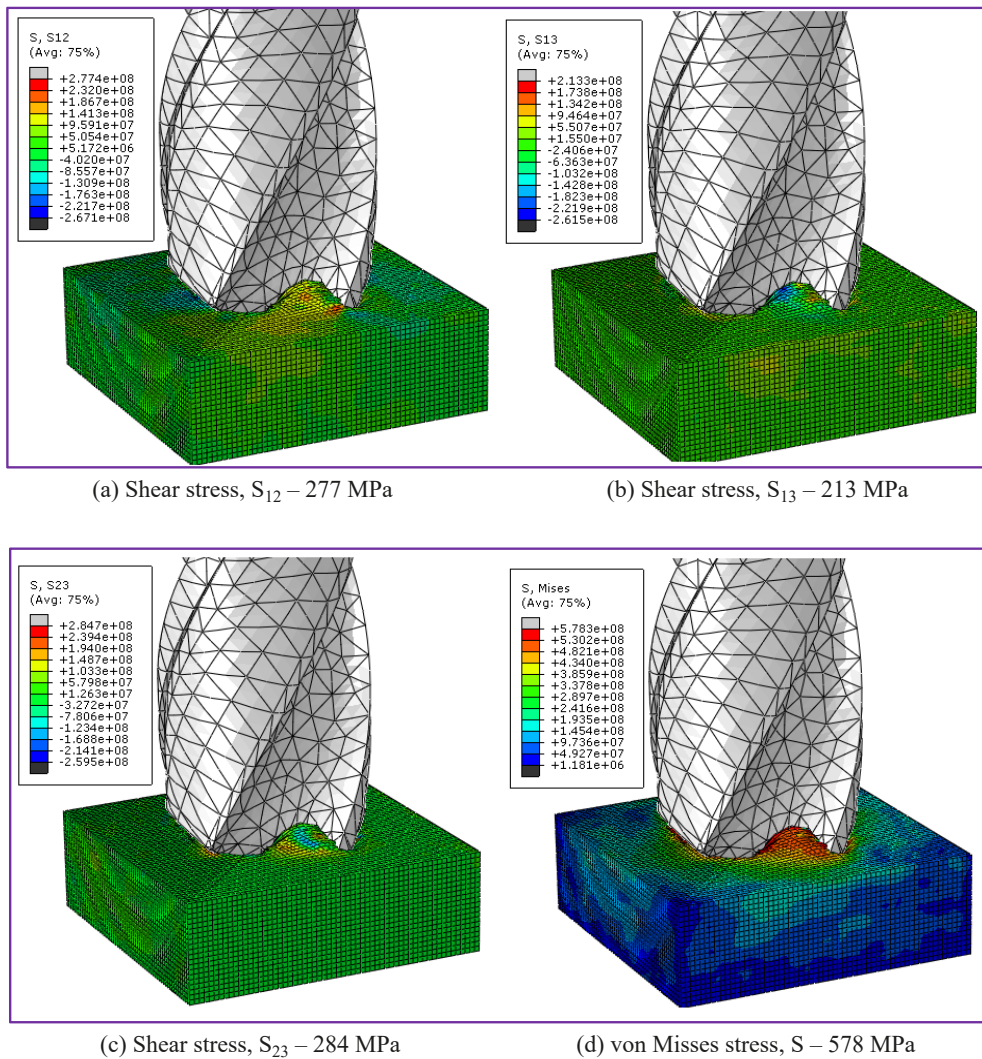


Fig. 8. Stress plot from 3D FEA results at N = 1500 rpm, Feed rate = 5 mm/min

ated due to the shearing action of the tool cutting edge with the MMC. The 3D FEM simulation result reveals the influences of shear stress on the chip creation process, chip morphology and the failure mode of the MMC. This necessitates to investigate on stress development during MMC drilling. From the 3D FE simulation results it is revealed that the shear stress S_{23} obtained is 284 MPa (shown in Fig. 8) which is comparatively more than the shear strength value given in TABLE 4 [42]. The von Misses stress, S observed is $S = 578$ MPa during the chip formation process.

3.3. Chip formation phenomenon in 3D FE simulation

Fig. 9(a)-(b) shows the images of the chip formation obtained from the simulation of 3D FEM while drilling the aluminium nanocomposite. The shearing action of the tool cutting

edge generates the chip which flows out through the spiral flute of the drill tool. Moreover, this phenomenon facilitates the formation of continuous spiral-shaped chips especially for a particular range of spindle speed (given in TABLE 1). Curling of the chip is observed because of the interaction of the chip with the rake surface of the drill tool [29]. The chip streams out of the MMC through the spiral flute, which is in the form of a lengthy curled spiral chip at a lower spindle speed <1000 rpm. The chip when comes into contact with the edges of the drill tool, hole edge and tool holder the chip breaking takes place. Fig. 10 shows how continuous spiral-shaped chips [43] are formed which are developed at lower spindle speed especially when the feed/rotation is >0.01 mm/rev (also shown in Fig. 11). When the selected spindle speed is >2000 rpm the chip formed is very tiny and segmented with lesser width. This information concludes that the size and shape of the drilled chips are very much affected by the cutting velocity and feed [44].

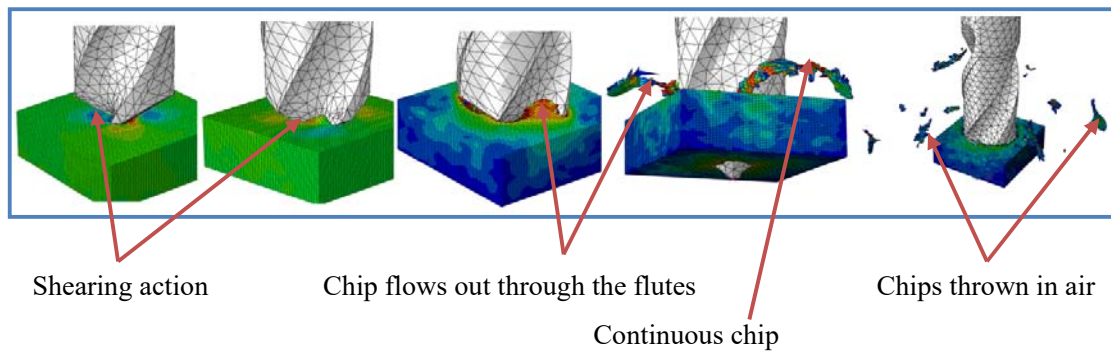


Fig. 9. (a) 3D FEA drilling simulation of chip formation at N = 1500 rpm, Feed rate = 5 mm/min

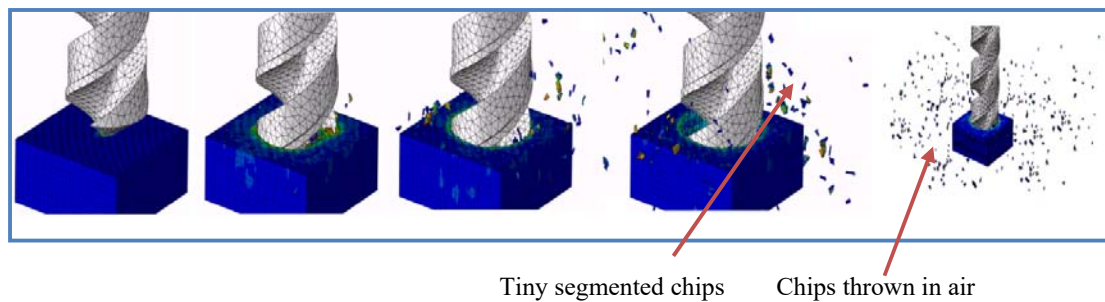


Fig. 9. (b) 3D FEA drilling simulation of chip formation at N = 3000 rpm, Feed rate = 5 mm/min

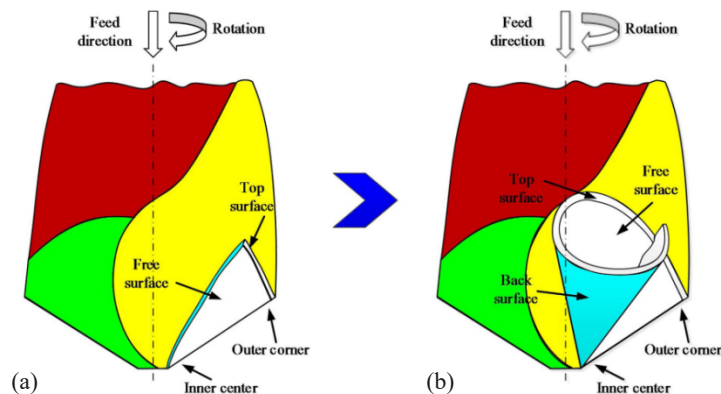


Fig. 10. 3D chip generation process in drilling operation (a) initial formation of chip (b) formation of spiral shape [37]

Using the step module in the ABAQUS software the workpiece model is discretized with the Arbitrary Lagrangian-Eulerian (ALE) adaptive meshing concept. This technique of meshing is commonly used for larger deformation problems which shows more element distortion and entanglement. Simulating the machining process is such a kind of problem which requires the ALE adaptive meshing technique to be incorporated into the workpiece model to avoid element distortion, material leaving away from the mesh, runtime errors and termination of the FE solver without solving the problem. The chip formation is initiated when the stiffness of the workpiece material degrades progressively with respect to the specified damage factors. The progressive damage criteria along with ALE adaptive mesh activates chip formation in a smoother way as shown in Fig. 9 [36,45].

3.4. Chip characteristics study of the chips collected from drilling experiments

In drilling operations, the interaction of the drill tool and the composite laminate is a complex mechanism which is mainly because of the geometrical complexity of the drill tool. Hence, it is very difficult to visualize and understand the chip formation process. However, chip formation, chip morphology and chip flow phenomenon highly influence on dimensional accuracy and drilled hole quality [44-47]. This creates the necessity to investigate the effects of process parameters such as spindle speed and feed rate on chip formation and removal and thereby improve the efficiency of the machining process. Moreover literature also reveals that the chip morphological investigations are very limited to orthogonal cutting processes, whereas only very few research works are reported in oblique cutting processes such as drilling and milling which is very much required in the current trend.

The chips collected from the drilling experimental studies with 18 different combinations of spindle speeds and feeds (given in TABLE 3) are displayed in Fig. 11. Fig. 11 also facilitates for making a detailed investigation on the influence of machining parameters over chip morphology. The images also reveal that the chip obtained from experimentation is of different thickness, width and length which is due to the effect of the selected combination of cutting parameters. The chip morphological studies reveal that the thickness of the drilled chip decreases with the increase of the spindle speed. Whereas, the length of the chip increases with the increase of spindle speed particularly at the feed rate 20 mm/min. The width of the chip decreases with the increase of cutting speeds. The chips are very fragile in nature when the thickness is very minimal, which is mainly influenced by feed per rotation (mm/rot) of the drill tool.

Long continuous spiral-shaped chips are formed which are developed at lower spindle speeds <1000 rpm and especially when the feed/rotation is >0.01 mm/rev. The formation of saw tooth is observed in the outer edge of the spiral shaped chips. The pitch distance of the spiral shaped chip reduces when the

feed rate increases, as shown in Fig. 11. At lower cutting speeds irrespective of feed rate, the thrust forces are higher. Moreover, the chip is mostly long continuous and spiral shaped with full width, this is the reason for elevated thrust forces, which are mainly required to curl the chip and form a continuous spiral shape. The chip thickness is also equally important for formation of long continuous spiral chip. Since, the chip thickness is comparatively higher when the spindle speed is low and at a feed rate ≥ 20 mm/min, this is the main reason for spiral chip formation and higher thrust force value.

Small continuous chips with lamella structure shown in Fig. 12(g) are collected while performing drilling at $N = 1000$ to 2000 rpm, particularly for feed rate ≤ 10 mm/min. Small continuous chips are obtained in this case since, the width of the chip obtained is lesser, on the other hand, the chip thickness obtained is more than enough to resist the breaking. The Figs. 11, 12(h) also reveals the formation of small curled chips when the spindle speed is >1500 rpm and the feed rate = 15 mm/min. This kind of chip morphology is observed when machining is done at moderate cutting speed and feed, which influences more on chip formation mechanism. The drilled chip curls due to the interaction of chip with the rake surface of the twist drill [38, 39]. Formation of crack, sawtooth and voids are seen which tend to produce chips with smaller length and width. Tiny segmented chips (shown in Fig. 12(i)) like flakes with multiple cracks were collected when the drilling process was carried out with a feed rate of 5 mm/min and 3000 rpm spindle speed as shown in Fig. 11. This is due to the effect of higher cutting speed, lower chip width and thickness since feed per rotation is much lesser at higher cutting speed and lower feed. Therefore, the thickness of the chip obtained is extremely thin followed by the shearing action of the cutting edge which facilitates the chip-breaking process very easily resulting in the formation of segmented tiny chips.

From Fig. 11, we can observe a significant influence of cutting speed and also feed on chip characteristics. The pitch distance of the spiral-shaped chip reduces when the feed rate increases. Fig. 12 displays the magnified ($5\times$) view of the chips obtained from drilling experiments. Figs. 12(a) and 12(b) shows the closer view of the chip at $N = 250$ rpm and at $f = 5, 10$ mm/min. The lengthy spiral-shaped continuous chips with cracks and sawtooth at the inner edge are seen for this particular cutting condition. The flow of the chip through the flute region is easy, slow and steady due to the lower cutting speed. Hence the chip does not break easily and the pitch value of the spiral shape is 6 to 7 mm. which is more when compared to the spiral chips obtained from other cutting conditions (shown in Fig. 10). Fig. 12(c) reveals the magnified view of chip morphology at $N = 250$ rpm, $f = 20$ mm/min, for this particular cutting condition the chip obtained, is thick continuous spiral-shaped without lamella structure. However, the presence of sawtooth is seen in the outer and also inner edges of the spiral shape. The pitch distance of the spiral shape is around 5 to 6 mm.

Fig. 12(d) shows the magnified view of the chip at $N = 1000$ rpm, $f = 10$ mm/min, for this particular machining condition the chip collected, is continuous and spiral-shaped with

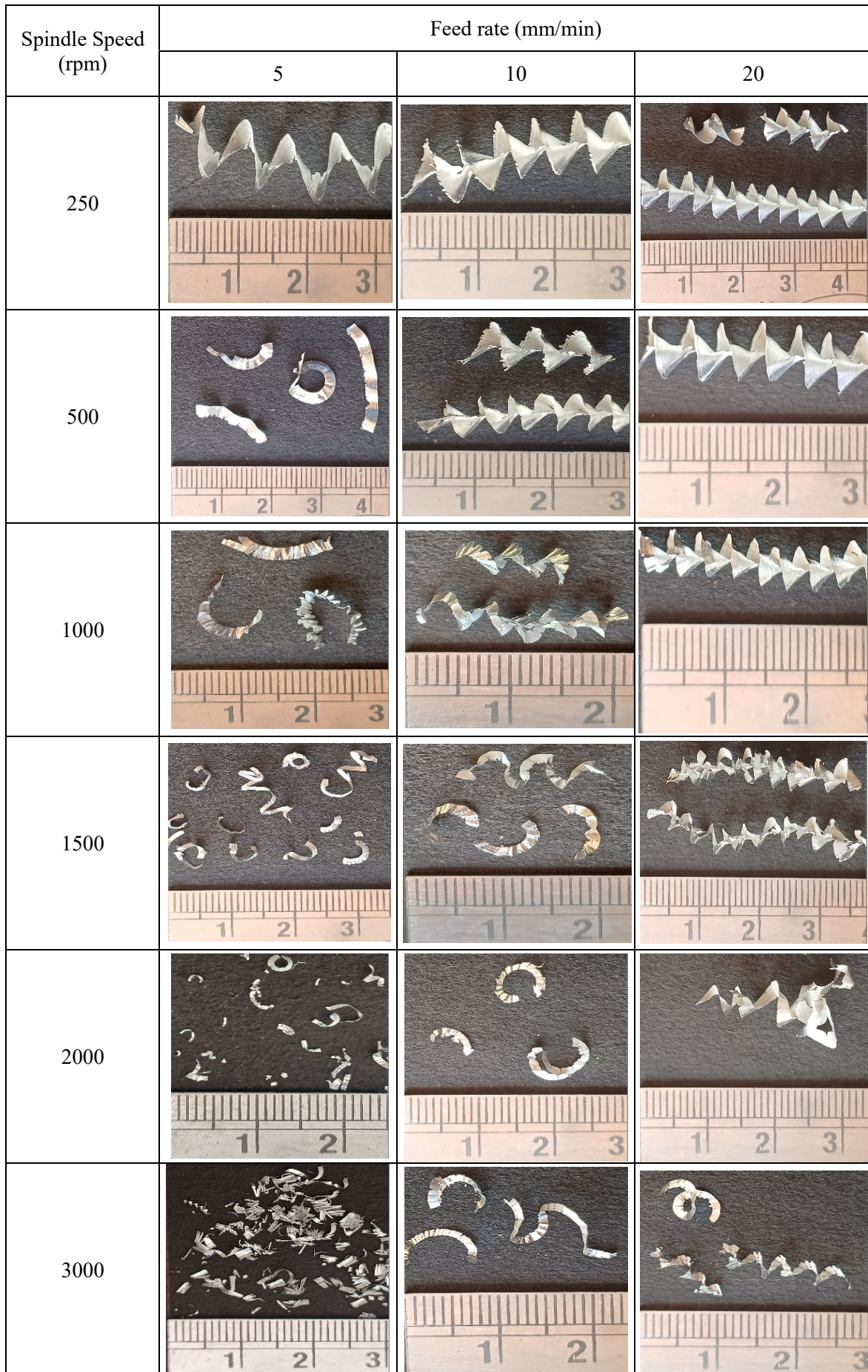


Fig. 11. Chip morphology of aluminium nanocomposite while drilling with different machining parameter combinations



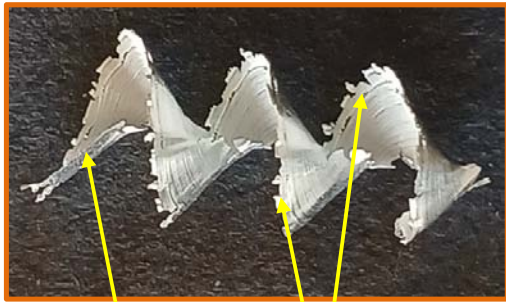
Long continuous spiral shaped chip

Cracks & Saw tooth

Long continuous spiral shaped chip

(a) $N = 250$ rpm, $f = 5$ mm/min

(b) $N = 250$ rpm, $f = 10$ mm/min



Continuous thick shaped chip

Saw tooth

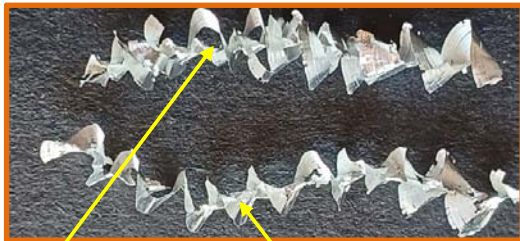
(c) $N = 250$ rpm, $f = 20$ mm/min



Continuous short thin spiral shaped chip spiral

Lamella structure

(d) $N = 1000$ rpm, $f = 10$ mm/min



Continuous thin distorted

Spiral shaped

(e) $N = 1500$ rpm, $f = 20$ mm/min



Spiral shaped chip with lesser width

Lamella structure with sawtooth & voids

(f) $N = 3000$ rpm, $f = 20$ mm/min



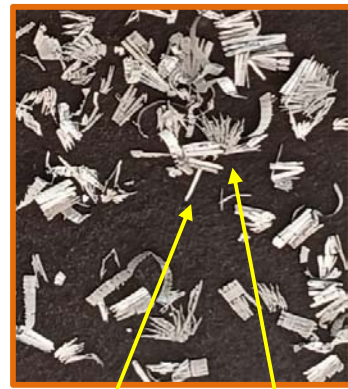
Continuous thin shaped chip with lamella structure

(g) $N = 1500$ rpm, $f = 5$ mm/min



Short very thin shaped curled chip with cracks & voids

(h) $N = 1500$ rpm, $f = 5$ mm/min



Tiny segmented chips like flakes with multiple cracks

(i) $N = 3000$ rpm, $f = 5$ mm/min

Fig. 12. Experimental chip characteristics at different cutting Speeds and feeds

a more lamella structure. From this, it is evident that continuous chips will not be developed for spindle speeds >1000 rpm. Since, the formation of lamella structure induces chip breaking if the thickness of the chip is lesser, which is also observed during experimentation as shown in Fig. 10. The chip image shown in Fig. 12(e) is captured at $f = 20$ mm/min and $N = 1500$ rpm. The irregular and distorted spiral-shaped chips are obtained as an effect of a comparatively higher feed rate and spindle speed combination. The chip thickness is also lesser when compared to Fig. 12(a)-(b). The pitch distance of the spiral shape reduces and is in the range of 4 to 5 mm. Fig. 12 (f) is captured for $f = 20$ mm/min and $N = 3000$ rpm. The chip obtained is short continuous spiral-shaped and extremely thin with lamella structure.

The chip obtained is very fragile since it is extremely thin and moreover, the presence of sawtooth and voids are also observed.

3.5. Chip Morphology – Experimental Vs FEA

Fig. 13 shows the images of the chips collected from the drilling experiments and from the 3D FE Model simulation outcomes. The chip images show excellent similarity in terms of chip characteristics. It also discloses the existence of cracks, lamella, voids and saw tooth. The chip images captured from 3D FEM simulation outcomes agreed well with the experimental chip images which evidences the ability and reliability of the

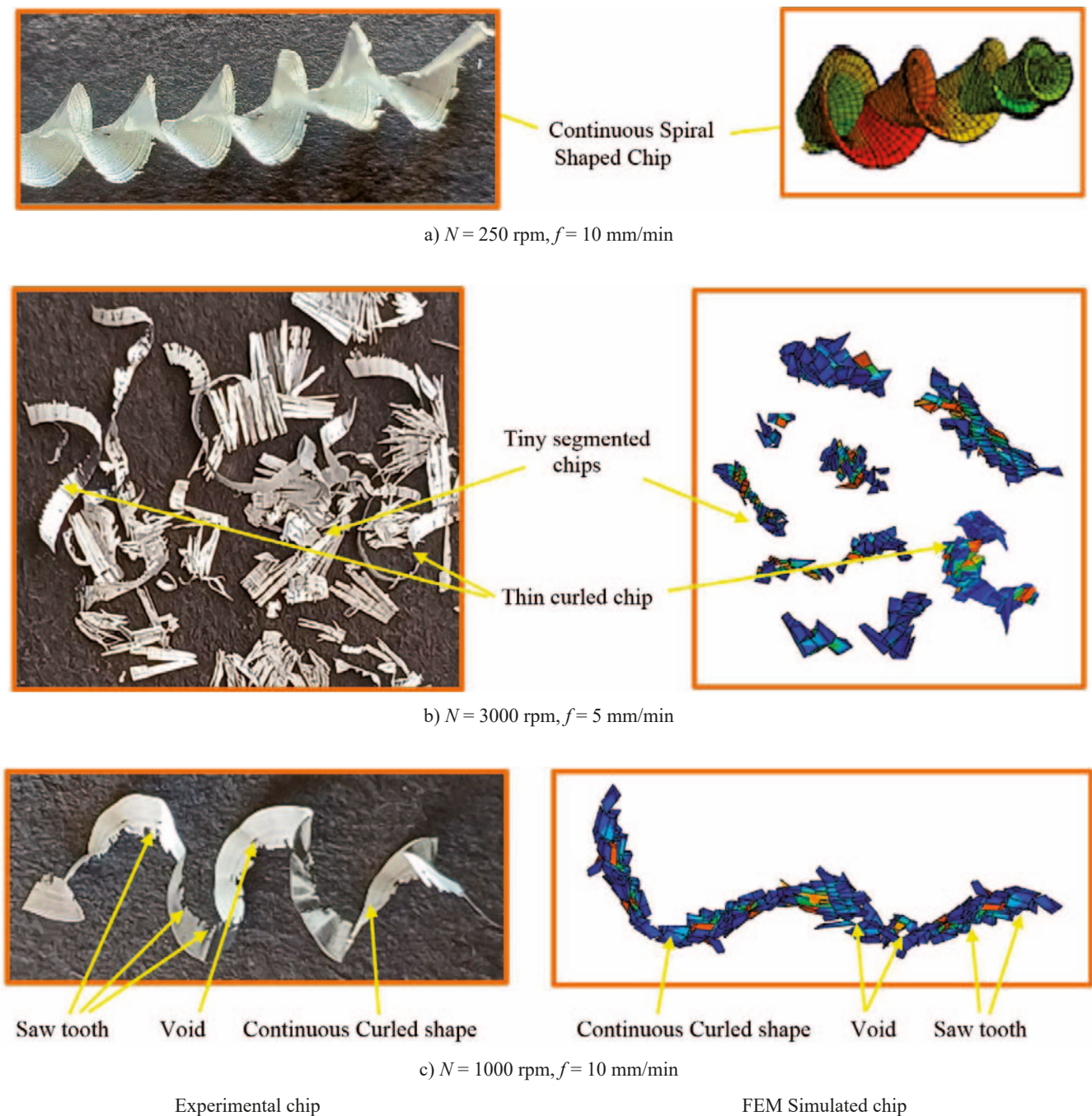


Fig. 13. Correlation of chips characteristics obtained from experimental results and 3D FEM simulation results

developed 3D FEM in forecasting the morphology of the chip in the drilling process.

3.6. Hole quality analysis

The experimental drilling is carried out with different cutting speeds and feed combinations listed in Fig. 11. The images of the drilled holes obtained from 3D FEM simulation results are shown in Fig. 14. Fig. 15 shows the drilled holes in the fabricated MMC from experimentation. The drilled surface of drilling experiment no. 1 (low feed = 5 mm/min and cutting speed = 250 rpm) shows more surface roughness, burrs and scratches, which is due to the influence of the selected process parameters. The reinforcement particle which is harder to break, slides over during cutting action and it also influences the surface roughness. The lower rate of chip formation in this case also influences the surface quality of the drilled hole. Whereas for the same feed rate of 5 mm/min and at cutting speed = 3000 rpm (Experiment no. 6), the surface quality of the drilled hole is relatively better.

At feed rate = 20 mm/min and cutting speed = 250 rpm (Experiment no. 13), the drilled surface shows lesser markings

without burrs. The surface roughness is relatively very minimal when compared to experiment no. 1. Whereas at higher feed and cutting speed, when the selected feed rate = 20 mm/min and cutting speed = 3000 rpm (Experiment no. 16) the surface finish is far better when compared to all other shown in Fig. 13. The above points infer the influence of process parameters on machining quality [44].

4. Conclusion

The 3D FEM developed in this research work simulates and reveals the insight of the drilling process in aluminium nanocomposite. The results acquired from the experimental drilling and 3D FEM simulation are compared to validate the developed 3D FE Model. This validated 3D FE model was suggested and proposed to perform simulation studies in drilling of the aluminium nanocomposites for predicting the critical thrust force and chip characteristics.

The critical thrust forces are recorded from experimental and 3D FE simulation results and it is correlated. The correlation is found to be in good agreement with the deviation of 10 to 15%. The critical thrust forces (F_z) decrease when the cutting speed

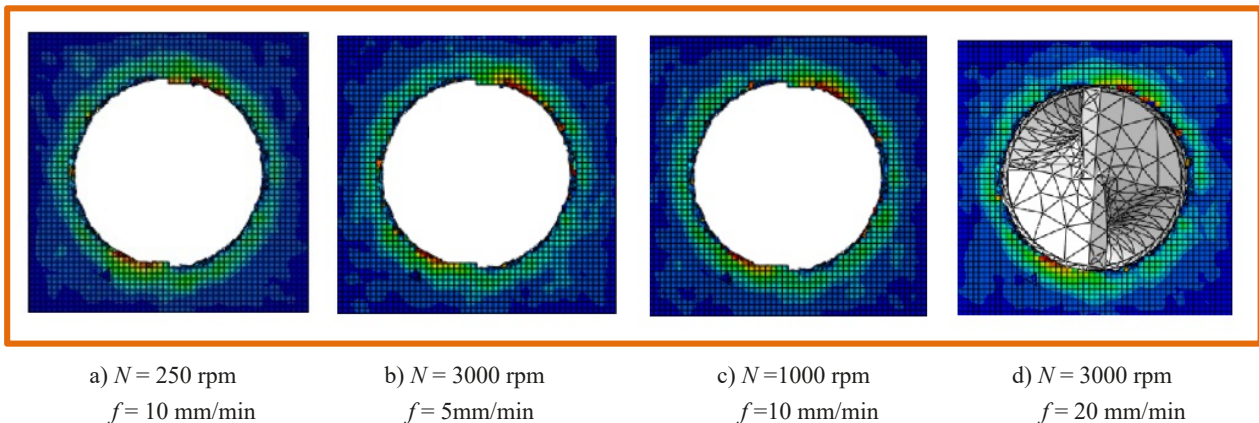


Fig. 14. Images of the drilled holes from 3D FEM simulation results



Fig. 15. Quality of the drilled surface

is increased. However, increasing the feed rate leads to a rise in critical thrust force. The research work reports a maximum critical thrust force of 716 N at $V_c = 7.85$ m/min and $f = 20$ mm/min. Therefore, it is suggested to drill this aluminium nanocomposite with a lower feed and higher cutting velocity to minimize the drilling-induced damages caused by elevated thrust force.

The chip images collected from drilling experiments and 3D FEM simulation show a variety of chip morphology with respect to cutting speed and feeds such as long continuous spiral-shaped, short continuous thin spiral-shaped, spiral-shaped with lamella structure, continuous thin distorted spiral-shaped and segmented chips like flakes. The presence of cracks, voids, sawtooth and lamella structure is observed from the chip morphological investigation. The correlation of chip images captured from experimental and 3D FEM simulation is good and reliable.

The stress plots captured from the 3D FEM drilling simulation shows; maximum Shear stress of 284 MPa and von Mises stress of 578 MPa in the cutting zone during chip formation and it is also comparable with the shear strength and ultimate strength of the aluminium nanocomposite. The drilled chip images show the failure phenomenon of the aluminium nanocomposite during drilling. The surface quality of the drilled hole is better when drilling is performed at a higher cutting speed, which is suggested for future investigations.

Furthermore, by utilizing this 3D FE Model, it is proposed to extend the current research work on the drilling and milling of aluminium-based MMC's and FRP's with other failure models. Since, applications of aluminium based MMC's are extensively increasing in the modern day industries for making light weight products with high strength and reliability.

Acknowledgements

The authors thank the Department of Production Technology, Madras Institute of Technology, Chrompet, Chennai, India for providing the Laboratory and Testing Facility.

REFERENCES

- [1] R.El Alaiji, L. Lasri, A. Bouayad, 3D finite element modelling of chip formation and induced damage in machining of fiber reinforced composites. *American Journal of Engineering Research* **4** (7), 123-132 (2015).
- [2] V.A.Phadns, A. Roy, V.V. Silberschmidt, Finite element analysis of drilling in carbon fiber reinforced polymer composites. IOP Publishing. *Journal of Physics: Conference Series*. **382** (2012). DOI: <https://doi.org/10.1088/1742-6596/382/1/012014>
- [3] Vikas Dhawan, Kishore Debnath, Prediction of Forces during Drilling of Composite Laminates Using Artificial Neural Network: A New Approach. *FME Transactions* **44** (1), 36-42 (2016). DOI: <https://doi.org/10.5937/fmet1601036D>
- [4] R. Bach, Aluminium in transport; 2020. <https://www.aluminium-leader.com/application/transport/> [accessed 16th August 2024].
- [5] H. Liu, W. Zhu, H. Dong, Y. Ke, A helical milling and oval countersinking end-effector for aircraft assembly. *Mechatronics* **46**, 101-114 (2017). DOI: <https://doi.org/10.1016/j.mechatronics.2017.07.004>
- [6] Oğuz Çolak, Talha Sunar, Cutting Forces and 3D Surface Analysis of CFRP Milling with PCD Cutting Tools. *Elsevier Procedia CIRP*. **45**, 75-78 (2016). DOI: <https://doi.org/10.1016/j.procir.2016.03.091>
- [7] S. Ghafarizadeh, Jean-Francois Chatelain, Gilbert Lebrun, Finite element analysis of surface milling of carbon fiber-reinforced composites. *International Journal of Advanced Manufacturing Technology* **87**, 399-409 (2016). DOI: <https://doi.org/10.1007/s00170-016-8482>
- [8] J.Y. Sheikh-Ahmad Machining of Polymer Composites. Springer, New York (2009). DOI: <https://doi.org/10.1007/978-0-387-68619-6>
- [9] İ. Ucun, 3D finite element modelling of drilling process of Al7075-T6 alloy and experimental validation. *Journal of Mechanical Science and Technology* **30** (4), 1843-1850 (2016). DOI: <https://doi.org/10.1007/s12206-016-0341-0>
- [10] X. Soldani, C. Santiuste, A. Muñoz-Sánchez, M. Miguélez, Influence of tool geometry and numerical parameters when modeling orthogonal cutting of LFRP composites. *Composites Part A – Applied Science and Manufacturing* **42** (9), 1205-1216 (2011). DOI: <https://doi.org/10.1016/j.compositesa.2011.04.023>
- [11] M. Aamir, K. Giasin, M. Tolouei-Rad, A. Vafadar, A review: Drilling performance and hole quality of aluminium alloys for aerospace applications. *Journal of Materials Research and Technology* **9** (6), 12484-12500 (2020). DOI: <https://doi.org/10.1016/j.jmrt.2020.09.003>
- [12] D. Sun, P. Lemoine, D. Keys, P. Doyle, S. Malinov, Q. Zhao, Hole-making processes and their impacts on the microstructure and fatigue response of aircraft alloys. *Int Journal of Advanced Manufacturing Technology* **94** (5-8), 1719-26 (2011). DOI: <https://doi.org/10.1007/s00170-016-9850-3>
- [13] Khaled Giasin, Sabino Ayyar-Soberanis, Toby French, Vaibhav Padnis, 3D finite Element Modelling of cutting forces in drilling fibre Metal laminates and experimental hole quality analysis. *Appl Compos Mater*. (2016). DOI: <https://doi.org/10.1007/s10443-016-9517-0>
- [14] K.S. Vijay Sekar, M. Pradeep Kumar, Finite element simulations of Ti6Al4V titanium alloy machining to assess material model parameters of the Johnson-Cook constitutive equation. *Journal of the Brazilian Society of Mechanical Sciences and Engineering* **33** (2), 203-21 (2011). DOI: <https://doi.org/10.1590/S1678-58782011000200012>
- [15] K. Giasin, A. Hodzic, V. Phadnis, S. Ayvar-Soberanis, Assessment of cutting forces and hole quality in drilling Al2024 aluminium alloy: experimental and finite element study. *The International Journal of Advanced Manufacturing Technology* **87** (5), 2041-2061 (2016). DOI: <https://doi.org/10.1007/s00170-016-8563-y>
- [16] N. Yaşar, Thrust force modelling and surface roughness optimization in drilling of AA-7075, FEM and GRA. *J. Mech. Sci. Technol.* **33**, 4771-4781 (2019). DOI: <https://doi.org/10.1007/s12206-019-0918-5>

- [17] R. Bhushan, Effect of SiC particle size and weight% on mechanical properties of AA7075 SiC composite. *Advanced Composites and Hybrid Materials* **4**, 1-12 (2021).
DOI: <https://doi.org/10.1007/s42114-020-00175-z>
- [18] S. Rasaei, A.H. Mirzaei, D. Almasi, Constitutive modelling of Al7075 using the Johnson-Cook model. *Bull. Mater. Sci.* **43** (23) (2020).
DOI: <https://doi.org/10.1007/s12034-019-1987-x>
- [19] P. Kumar, B.V. Kumar, R. Joshi, T.H. Manjunatha, Evaluation of Al7075 reinforced with SiC for its mechanical properties & surface roughness by drilling. *Materials Today: Proceedings* **5** (11), 25121-25129 (2018).
DOI: <https://doi.org/10.1016/j.matpr.2018.10.313>
- [20] S. Senthil Babu, C. Dhanasekaran, G. Anbuezhayan, Kumaran Palani, Parametric analysis on drilling of aluminium alloy hybrid composites reinforced with SiC/WC. *Eng. Res. Express.* **4**, 025036 (2022). DOI: <https://doi.org/10.1088/2631-8695/ac7038>
- [21] Samadhan Deshmukh, Girish Joshi, Asha Ingle, Dineshsingh Thakur, An overview of Aluminium Matrix Composites: Particulate reinforcements, manufacturing, modelling and machining. *Materials Today: Proceedings* **46** (17), 8410-8416 (2021).
DOI: <https://doi.org/10.1016/j.matpr.2021.03.450>
- [22] L. Zhou, C. Cui, P. Zhang, Finite element and experimental analysis of machinability during machining of high-volume fraction SiCp/Al composites. *Journal of Advanced Manufacturing Technology* **91**, 1935-1944 (2017).
DOI: <https://doi.org/10.1007/s00170-016-9933-1>
- [23] Yong He, Jun Zhang, Yutong Qi, Hongguang Liu, Afaq R. Memon, Wanhua Zhao, Numerical study of microstructural effects on chip formation in high speed cutting of ductile iron with discrete element method. *Journal of Materials Processing Technology* **249**, 291-301 (2017).
DOI: <https://doi.org/10.1016/j.jmatprotec.2017.06.006>
- [24] X. Geng, W. Dou, J. Deng, Z. Yue, Simulation of the cutting sequence of AISI 316L steel based on the smoothed particle hydrodynamics method. *The International Journal of Advanced Manufacturing Technology* **89** (1-4), 643-650 (2016).
DOI: <https://doi.org/10.1007/s00170-016-9116-0>
- [25] J.M. Carbonell, J.M. Rodríguez, E. Oñate, Modelling 3D metal cutting problems with the particle finite element method. *Comput. Mech.* **66**, 603-624 (2020).
DOI: <https://doi.org/10.1007/s00466-020-01867-5>
- [26] John A. Nairn, Numerical simulation of orthogonal cutting using the material point method. *Engineering Fracture Mechanics* **149**, 262-275 (2015).
DOI: <https://doi.org/10.1016/j.engfracmech.2015.07.014>
- [27] C. Prakash, K.S.V. Sekar, 3D Finite Element Analysis of Drilling of Glass Fiber Reinforced Polymer Composites. *Adv. Sci Eng. Med.* **10**, 308-312 (2018).
DOI: <https://doi.org/10.1166/ asem.2018.2125>
- [28] C. Prakash, K.S. Vijay Sekar, 3D Finite Element Analysis of Slot Milling of Unidirectional Glass Fiber Reinforced Polymer Composites. *Journal of the Brazilian Society of Mechanical Sciences and Engineering* **40** (2018).
DOI: <https://doi.org/10.1007/s40430-018-1195-4>
- [29] C. Prakash, K.S. Vijay Sekar, Finite Element Analysis of the slot milling of Carbon Fiber Reinforced Polymer composites. *IOP Conf. Ser.: Mater. Sci. Eng.* **1128**, 012050 (2021).
DOI: <https://doi.org/10.1088/1757-899X/1128/1/012050>
- [30] C. Prakash, K.S. Vijay Sekar, Influence of Friction Coefficient and Failure Model in 3D FEA Simulation of Drilling of Glass Fiber Reinforced Polymer Composites. In: K. Vijay Sekar, M. Gupta, A. Arockiarajan (eds.). *Advances in Manufacturing Processes. Lecture Notes in Mechanical Engineering* (2019).
DOI: https://doi.org/10.1007/978-981-13-1724-8_8
- [31] J. Prakash, S. Gopalakannan, V.K. Chakravarthy, Mechanical characterization studies of aluminium alloy 7075 based nanocomposites. *Silicon* **14** (4), 1683-1694 (2022).
DOI: <https://doi.org/10.1007/s12633-021-00979-8>
- [32] J. Prakash, S. Gopalakannan, Teaching – learning-based optimization coupled with response surface methodology for micro electrochemical machining of aluminium nanocomposite. *Silicon* **13** (2), 409-432 (2021).
DOI: <https://doi.org/10.1007/s12633-020-00434-0>
- [33] C. Prakash, J. Prakash, Investigation and selection of optimistic material for two wheeler brake disc – An Experimental and Finite Element Approach, *Proceeding of IMech D – Automobile Engineering – Sage Journals* (2024).
DOI: <https://doi.org/10.1177/09544070241254148>
- [34] C. Prakash, K.S. Vijay Sekar, 3D Finite Element Analysis of Slot Milling of Carbon Fiber Reinforced Polymer Composite. *Journal of the Balkan Tribological Association* **23** (3), 497-514 (2017).
- [35] C. Prakash, A. Arockia Selvakumar, J. Prakash, FEA in high speed milling of AA7075 reinforced with nB₄Cp. *AIP Conf. Proc.* **29** July 2024, **3216** (1), 040002 (2024).
DOI: <https://doi.org/10.1063/5.0226489>
- [36] D. Simulia, Abaqus 6.14 User's manual. Dassault systems, Providence, RI (2014). <http://50.16.225.63/v6.14/>
- [37] CATIA V5R14, User Manual, Dassault systems, Providence, RI (2014).
https://www.maruf.ca/files/catiahelp/CATIA_P3_default.htm
- [38] M.S Won, CKH. Dharan, Chisel edge and pilot hole effects in drilling composite laminates. *J. Manuf. Sci. Eng.* **124** (2), 242-247 (2002). DOI: <https://doi.org/10.1115/1.1448317>
- [39] K. Anand, M.V. Siddharth, K.S. Vijay Sekar, S. Suresh kumar, Impact of tool inserts in high speed machining of GFRP composite material. *Applied Mechanics and Materials* **787**, 664-668 (2015).
DOI: <https://doi.org/10.4028/www.scientific.net/AMM.787.664>
- [40] I. Singh, N. Bhatnagar, Drilling-induced damage in uni-directional glass fiber reinforced plastic (UD-GFRP) composite laminates. *International Journal of Advanced Manufacturing Technology* **27**, 877-882 (2006).
DOI: <https://doi.org/10.1007/s00170-004-2282-5>
- [41] I. Singh, N. Bhatnagar, P. Viswanath, Drilling of uni-directional glass fiber reinforced plastics: Experimental and finite element study. *Materials and Design* **29**, 546-553 (2007).
DOI: <https://doi.org/10.1016/j.matdes.2007.01.029>
- [42] C. Prakash, K.S. Vijay Sekar, 3D Finite Element Analysis Simulation of Slot Milling Process for Titanium Alloy Ti6Al4V. *International Conference on Progressive Research In Applied Sciences*,

- Engineering and Technology, ICPRASET 2K18, IOSR Journal of Engineering 22-28 (2018).
<https://www.iosrjen.org/Papers/ICPRASET%20K18/surya/Volume%201/auto/5.%2022-28.pdf>
- [43] Zhaoju Zhu, Kai Guo, Jie Sun, Jianfeng Li, Yang Liu, Lei Chen, Yihao Zheng, Evolution of 3D chip morphology and phase transformation in dry drilling Ti6Al4V alloys. *Journal of Manufacturing Processes* **34**, Part A, 531-539 (2018).
DOI: <https://doi.org/10.1016/j.jmapro.2018.07.001>
- [44] C. Prakash, A. Arockia Selvakumar, K.S. Vijay Sekar, 3D Finite Element investigation in high speed drilling of unidirectional Glass Fiber Reinforced Polymer composite. *Materials Today: Proceedings* (2023). DOI: <https://doi.org/10.1016/j.matpr.2023.08.234>
- [45] G. Johnson, W. Cook, Fracture characteristics of three metals subjected to various strains, strain rates, temperatures and pressures. *Engineering Fracture Mechanics* **21** (1), 31-48 (1985).
DOI: [https://doi.org/10.1016/0013-7944\(85\)90052-9](https://doi.org/10.1016/0013-7944(85)90052-9)
- [46] A.I. Azmi, Chip formation studies in machining fibre reinforced polymer composites. *Int. J. Materials and Product Technology* **46** (1), 32-46 (2013).
DOI: <https://doi.org/10.1504/ijmpt.2013.052790>
- [47] C. Prakash, 3D Finite Element Analysis in Drilling of Unidirectional Carbon Fiber Reinforced Polymer Composite. *International Journal on Interactive Design and Manufacturing* (2024).
DOI: <https://doi.org/10.1007/s12008-024-02089-2>